



HAL
open science

SCIAMACHY Absorbing Aerosol Index ? calibration issues and global results from 2002?2004

M. de Graaf, P. Stammes

► **To cite this version:**

M. de Graaf, P. Stammes. SCIAMACHY Absorbing Aerosol Index ? calibration issues and global results from 2002?2004. Atmospheric Chemistry and Physics, 2005, 5 (9), pp.2385-2394. hal-00295738

HAL Id: hal-00295738

<https://hal.science/hal-00295738>

Submitted on 18 Jun 2008

HAL is a multi-disciplinary open access archive for the deposit and dissemination of scientific research documents, whether they are published or not. The documents may come from teaching and research institutions in France or abroad, or from public or private research centers.

L'archive ouverte pluridisciplinaire **HAL**, est destinée au dépôt et à la diffusion de documents scientifiques de niveau recherche, publiés ou non, émanant des établissements d'enseignement et de recherche français ou étrangers, des laboratoires publics ou privés.

SCIAMACHY Absorbing Aerosol Index – calibration issues and global results from 2002–2004

M. de Graaf and P. Stammes

Royal Netherlands Meteorological Institute, P.O. Box 201, 3730 AE De Bilt, The Netherlands

Received: 14 February 2005 – Published in Atmos. Chem. Phys. Discuss.: 26 May 2005

Revised: 29 July 2005 – Accepted: 2 September 2005 – Published: 15 September 2005

Abstract. The validity of the Absorbing Aerosol Index (AAI) product from the SCanning Imaging Absorption SpectroMeter for Atmospheric Cartography (SCIAMACHY) is discussed. The operational SCIAMACHY AAI product suffers from calibration errors in the reflectance as measured by SCIAMACHY and neglect of polarisation effects in the AAI computational algorithm. Therefore, the AAI product was recalculated, compensating for the errors, with reflectance data from the start of measurements of SCIAMACHY until December 2004. Appropriate correction factors were determined for the UV to correct for the radiometric error in the SCIAMACHY reflectances. The algorithm was provided with LookUp Tables in which a good representation of polarisation effects was incorporated, as opposed to the LookUp Tables of the operational product, in which polarisation effects were not accounted for. The results are presented, their validity discussed, and compared to the operational product and independent AAI data from the Total Ozone Mapping Spectrometer (TOMS). The AAI is very sensitive to calibration errors and can be used to monitor calibration errors and changes. The AAI is sensitive to sunglint and a correction flag used for the AAI is presented. From 2004 onwards, the new SCIAMACHY AAI is suitable to add to the continuation of the long-term AAI record. Important changes in the long-term AAI record due to instrument and algorithm changes are highlighted. Recommendations are given for improvement of the operational AAI product.

1 Introduction

The AAI is a dimensionless index indicating the presence of ultraviolet (UV)-absorbing aerosols in the Earth's atmosphere (Herman et al., 1997; Torres et al., 1998; De Graaf

et al., 2005). The AAI has been used for a long time in remote sensing to indicate UV-absorbing aerosols, like desert dust (e.g. Chiapello et al., 1999; Alpert and Ganor, 2001; Pandithurai et al., 2001; Spichtinger et al., 2001; Prospero et al., 2002; Moulin and Chiapello, 2004) and biomass burning aerosols (e.g. Hsu et al., 1996, 1999; Gleason et al., 1998; Duncan et al., 2003; Darmenova et al., 2005) over both land and oceans.

Initially developed as an error estimate in the TOMS ozone retrieval algorithm (Herman et al., 1997; Torres et al., 1998), the AAI records have become the longest records of global aerosol measurements available. Starting with Nimbus-7/TOMS in 1978, American TOMS instruments have provided daily global aerosol maps continuously for over 25 years, with a data gap only between May 1993 and June 1996. From 1995, the European ERS-2/GOME provided additional and independent AAI information, adding to the continuity of the AAI record and validity of the AAI as an aerosol detection quantity (De Graaf et al., 2005). Now, Envisat/SCIAMACHY results will be added to the AAI records.

Operational data production of SCIAMACHY started at the end of July 2002. Several improvements and changes of the data processor and key data characteristics followed in the subsequent two and a half years. In this paper, the operational AAI product of this period is presented briefly.

Improper characterisation of the instrument's response functions (key data) results at the moment in calibration errors in the measured reflectances of SCIAMACHY of up to 20%. This yields AAI errors in the order of 4–6, which is about 100% of the signal (De Graaf and Stammes, 2002). In this paper, correction factors for the reflectances are used and their validity for the calculation of AAI is investigated.

The operational AAI product is calculated using pre-calculated LookUp Tables (LUTs) of theoretical reflectances in a cloud-free and aerosol-free atmosphere. These LUTs were constructed with a radiative transfer model (Spurr and

Correspondence to: M. de Graaf
(graafdem@knmi.nl)

Balzer, 2000) which neglected polarisation effects. Here, the AAI is further improved using LUTs in which linear polarisation is accounted for. The effects of this are presented and discussed.

The result of the changes mentioned above is an off-line AAI algorithm using calibrated SCIAMACHY reflectances, off-line LUTs, and additional calibration constants, producing SCIAMACHY scientific AAIs. All off-line products developed after launch of the ENVISAT spacecraft are termed scientific products, to distinguish them from the operational products owned by ESA, and can be found at <http://www.sciamachy-validation.org>. The scientific AAI is presented and investigated, and compared to the operational product and other independent aerosol data.

This paper continues with a brief summary of the theory behind the AAI (Sect. 2). The characteristics of SCIAMACHY are described (Sect. 3), followed by a description of the operational AAI product and its shortcomings (Sect. 3.1). Improvements for an off-line product are discussed, leading to a new algorithm for a scientific AAI (Sect. 3.2), the results of which are laid out in Sect. 4. The spatial and temporal patterns of global aerosols found in the data are discussed and compared to TOMS AAI data. Sun glint and other problems in the data, related to the specific definition of the AAI, are pointed out. Finally, the results are discussed and some recommendations for future improvements are given (Sect. 5).

2 Absorbing Aerosol Index

The Absorbing Aerosol Index (AAI) is a measure for the spectral contrast between the reflectance of the real atmosphere-surface system, that may be affected by the presence of UV-absorbing aerosols, and that of a modelled atmosphere-surface system, that does not contain UV-absorbing aerosols. The modelled atmosphere may contain scatterers (Rayleigh scattering molecules, non-absorbing aerosols and cloud particles, as well as absorbing gases) and is bounded below by a surface with a wavelength independent reflectivity. The AAI is defined as the positive part of the residue, where the residue r is defined as (Herman et al., 1997)

$$r_{\lambda} = -100 \cdot \left\{ {}^{10}\log \left(\frac{R_{\lambda}}{R_{\lambda_0}} \right)^{\text{meas}} - {}^{10}\log \left(\frac{R_{\lambda}}{R_{\lambda_0}} \right)^{\text{Ray}} \right\}. \quad (1)$$

R_{λ} is the reflectance at a wavelength λ . R^{meas} is the measured reflectance in the atmosphere with aerosols, as opposed to a calculated reflectance in an aerosol-free atmosphere R^{Ray} , with only Rayleigh scattering and absorption by molecules and surface reflection and absorption. The reflectance is defined as $R = \pi I / (\mu_0 E_0)$, where I is the radiance at the top of the atmosphere (TOA), E_0 is the solar irradiance at TOA perpendicular to the direction of the incident sunlight and μ_0 is the cosine of the solar zenith angle θ_0 .

If the surface albedo A_s for the Rayleigh atmosphere calculation is chosen so that

$$R_{\lambda_0}^{\text{meas}} = R_{\lambda_0}^{\text{Ray}}(A_s), \quad (2)$$

where λ_0 is a reference wavelength, Eq. (1) can be reduced to

$$r_{\lambda} = -100 \cdot {}^{10}\log \left(\frac{R_{\lambda}^{\text{meas}}}{R_{\lambda}^{\text{Ray}}} \right), \quad (3)$$

where R_{λ}^{Ray} is calculated for surface albedo $A_s(\lambda_0)$, so the surface albedo is assumed to be constant in the range $[\lambda, \lambda_0]$. In this paper the traditional residue wavelength pair, $\lambda=340$ nm and $\lambda_0=380$ nm, is adopted.

On the assumption that the atmosphere is bounded from below by a Lambertian surface, which reflects incident radiation uniformly and unpolarised in all directions, the surface contribution to the reflectance at TOA can be separated from that of the atmosphere (Chandrasekhar, 1960):

$$R(\mu, \mu_0, \phi - \phi_0, A_s) = R_0(\mu, \mu_0, \phi - \phi_0) + \frac{A_s t(\mu) t(\mu_0)}{1 - A_s s^*}. \quad (4)$$

The first term, R_0 , is the path radiance, which is the atmospheric contribution to the reflectance. The second term is the contribution of the surface with an albedo A_s . t is the total atmospheric transmission, s^* is the spherical albedo of the atmosphere for illumination from below, μ is the cosine of the viewing zenith angle θ and $\phi - \phi_0$ is the relative azimuth angle. The path radiance R_0 is calculated with LUTs of $a_i(\mu, \mu_0)$, $t(\mu)$ and s^* for all wavelengths used. Then the surface albedo A_s in Eq. (2) can be found from

$$A_s = \frac{R - R_0}{t(\mu) t(\mu_0) + s^*(R - R_0)}, \quad (5)$$

by replacing R by $R_{\lambda_0}^{\text{meas}}$ in Eq. (5). Note that this equation allows negative surface albedos, which occurs for highly absorbing (aerosol) layers.

Sensitivity studies show (Torres et al., 1998; De Graaf et al., 2005) that UV-absorbing aerosols produce an effect on the spectrum that cannot be simulated with a pure Rayleigh atmosphere and an adjusted surface albedo, creating large, positive residues, even for wavelength independent aerosol refractive indices. Scattering effects are much better represented with a Rayleigh atmosphere and underlying adjusted surface albedo, yielding small, negative residues. The AAI is therefore defined as the positive part of the residue, thereby filtering clouds and scattering aerosols.

3 SCIAMACHY

SCIAMACHY is part of the payload of the European ‘‘Environment Satellite’’ Envisat, launched on 1 March 2002 onboard an Ariane-5 launch vehicle from the Guyana Space Centre into a polar orbit at about 800 km altitude, with an

equator crossing-time of 10:00 a.m. (local time) for the descending node, orbiting the Earth every 100 min. SCIAMACHY is a spectrometer designed to measure sunlight, transmitted, reflected and scattered by the Earth's atmosphere or surface in the ultraviolet, visible and near-infrared wavelength regions (240–2380 nm) at a moderate spectral resolution of 0.2–1.5 nm (Bovensmann et al., 1999). The radiance is observed in two alternating modes, nadir and limb, yielding data blocks called states. The nadir state swath is approximately $960 \times 490 \text{ km}^2$, and it is scanned from east to west in four seconds by rotation of one of the two internal mirrors. The result is a subdivision of the states into groundpixels of approximately $60 \times 30 \text{ km}^2$ at the optical integration time (IT) of 0.25 s. Longer integration times of 0.5 s and 1.0 s also occur, yielding groundpixels of $120 \times 30 \text{ km}^2$ and $240 \times 30 \text{ km}^2$. Even longer integration times occur, but they will not be considered here. The extra-terrestrial solar irradiance is measured each day, once per 14 orbits.

3.1 Operational AAI algorithm

SCIAMACHY's operational AAI product (L2-AAI) is calculated directly after downlinking of the data in the so-called near-real time level 1 (L1) to level 2 (L2) processing step. The processing steps are described in detail in Balzer et al. (2000). A brief summary is given here, to highlight the most important differences with the scientific AAI product, described below.

The reflectance is determined in the level 0 (L0) to L1 processing step for each groundpixel from channel 2, cluster 9, which contains the spectrum from 320.14 nm to 391.76 nm. Common normal mode ITs in cluster 9 are 0.25 s, 0.5 s and 1.0 s. These are constant within states, but can vary within orbits. The AAI is computed using the reflectances at 340 nm and 380 nm. A Rayleigh reflectance is determined from a pre-calculated LUT, for each pixel, dependent on geometry and surface height. The LUT has inputs for 11 reference heights from 0 to 5 km and 8 reference albedos from 0.0 to 0.9. The solar zenith angle θ_0 must be between 15° and 85° and the viewing zenith angle θ lower than 35° , otherwise no AAI is calculated.

The L2-AAI suffers from two major flaws. Firstly, the original LUTs were calculated with the use of a scalar radiative transfer model, so that polarisation was not accounted for in the Rayleigh scattering computations. When the LUTs were calculated, only a scalar version of the model, LIDORT (Spurr et al., 2001), was available. The residue calculations are sensitive to errors in the reflectances, see Fig. 1a. This figure shows the residue in a modelled Rayleigh atmosphere where polarisation has not been accounted for, for different geometries. In a Rayleigh atmosphere the residues should be exactly zero. The errors in the reflectance in the modelled atmosphere are of the order of about 10–15%, yielding erroneous residues of a maximum of -4 to 3.5 . New LUTs have

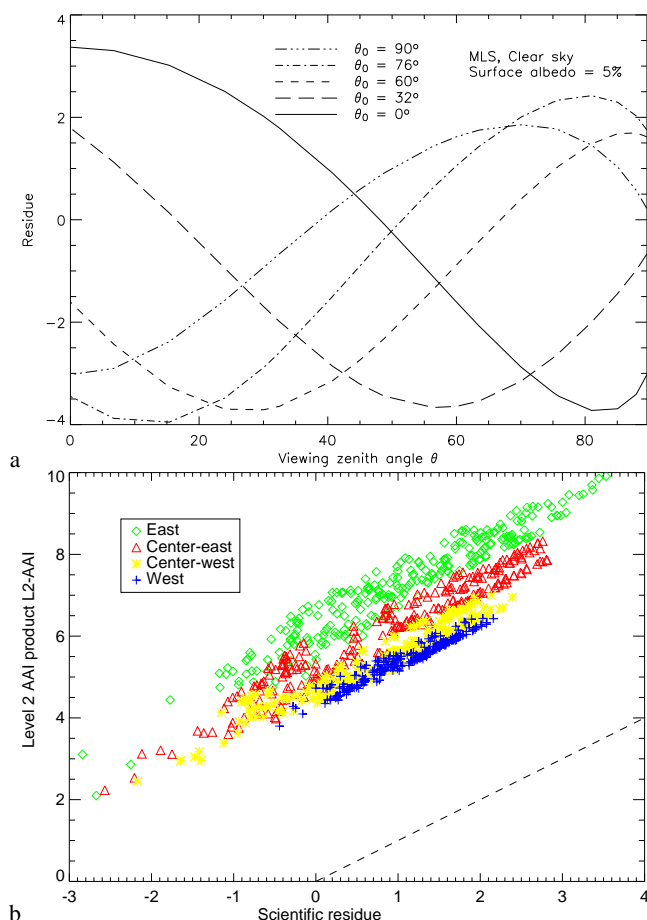


Fig. 1. (a) The residue in a modelled Rayleigh atmosphere where polarisation has not been accounted for as a function of viewing and solar zenith angles. Relative azimuth angle is zero. (b) The scientific residue compared to the operational level-2 AAI data for orbit 10969, states 5–9. The colours refer to pixels with approximately the same viewing geometry. The first four pixels of $30 \times 60 \text{ km}^2$ in a forward swath are called East pixels, the next 4 Center-east, the next 4 Center-west and the last 4 West pixels. The dashed line is the one-to-one line.

been created using a model that accounts for polarisation effects.

Secondly, the reflectances as measured by SCIAMACHY are underestimated in the UV by 10–20%, as reported by several workers (e.g. Tilstra et al., 2004). This results in an offset of the AAI of about 4–6 (De Graaf et al., 2004), which is of the order of the maximum expected AAI. To correct for these errors, a scientific AAI algorithm was constructed, which uses corrected SCIAMACHY L1 data (calibrated reflectances).

3.2 Scientific AAI algorithm

The scientific AAI (SC-AAI) is calculated off-line, i.e. after L1 data have been received via satellite link at the Royal

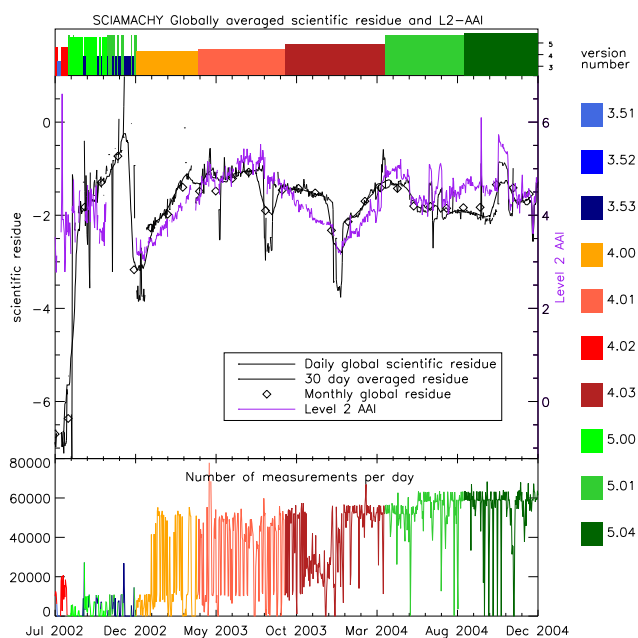


Fig. 2. Statistics of the off-line data as a function of time for the entire measurement period, 22 July 2002–31 December 2004. The uppermost panel and the colour codes denote the L1 processor version number of the data of a certain period. The central panel shows the data, averaged per day over the entire globe. The normal black line and individual points show the daily global averaged scientific residue. The bold black line is its 30 day running mean. The black diamonds show the monthly mean scientific residue. The purple line shows the L2-AAI (Note that the right axis is shifted by +6). The lower panel shows the number of pixels that were available for the scientific residue calculations per day.

Netherlands Meteorological Institute (KNMI). The data are calibrated and radiances and irradiances are extracted to determine the reflectances at 340 nm and 380 nm. These reflectances are averaged over a one nm wide window. After this, the reflectances are corrected for the underestimation of the reflectance by SCIAMACHY. This correction consists of a simple multiplication of the reflectances by a constant factor. Several factors were tried and the best multiplication factors were 1.210 for R_{340} and 1.130 for R_{380} (Tilstra et al., 2004). Note that different multiplication factors will lead to a linear shift in the resulting AAI (De Graaf et al., 2004, 2005).

The corrected reflectances are used in Eqs. (2) and (3). The inversion process and the LUTs used therein are described in detail in De Graaf et al. (2005). The LUTs were created using the Doubling-Adding KNMI (DAK) radiative transfer model (De Haan et al., 1987), in which polarisation is accounted for. The surface albedo is calculated directly using Eq. (5).

The changes are illustrated in Fig. 1b. This figure shows the scientific residue compared to the L2-AAI for 5 states of orbit 10969 on 5 April 2004 over the Sahara, where a dust plume was present at that time. Note that the sci-

entific residue is the quantity that is determined for all SCIAMACHY pixels. The SC-AAI is the quantity that signals the presence of aerosols, or other absorbing effects, by filtering of negative residues. The figure shows the offset of 4–6 of the L2-AAI compared to the scientific residue, caused by the underestimation of the reflectances. Moreover, it shows that the offset differs by about two for east and west pixels, which is caused by the neglect of polarisation in the L2-AAI. This behaviour is found throughout the data.

4 Results

The L2 data can be obtained from the European Space Agency (ESA). The scientific data are available at <http://www.temis.nl>. Both gridded daily data and gridded monthly means are available as well as daily and monthly pictures. The SC-AAI was determined from all SCIAMACHY L1 data available from 22 July 2002 to 31 December 2004.

The calibration processor of SCIAMACHY has regularly been updated over the last two and half years. This is reflected in the AAI data, which is very sensitive to calibration errors. In that way the AAI can be used as a monitor for calibration errors and improvements. This is illustrated in Fig. 2, which shows the number of pixels available at KNMI for the SC-AAI calculation, the processor version number that processed the L1 data of a certain period, and the results.

The uppermost panel and the colour code show the L1 processor version number, which reflects the status of the calibration process. Processor version 3.51 was the default when the first data became available. The processor was steadily updated to version 5.04 in December 2004, but re-processed data have replaced older versions frequently (the newest available data was always used). The lower panel shows the number of residues that have been determined in a day. Because a residue is computed for all pixels which have a reflectance at 340 nm and 380 nm, this is a good measure for the amount of SCIAMACHY data of a certain day available at KNMI. The centre panel of Fig. 2 shows the scientific residue, averaged daily over the globe, as the normal black line and some isolated dots. The bold black line is its 30 day running mean.

The daily global scientific residue was highly erratic in the beginning, ranging from -7 and lower to more than 0.5 . This is due to the very few number of measurements available at that time and the poor status of the calibration. Often, only one orbit was available on a day and the measurements frequently gave poor results. In 2004 the results improved considerably as the spread in the measurements decreased.

The monthly mean residues, averaged over the globe, are given as black diamonds. They are not exactly the same as the 30 day running mean, mainly because the monthly means are first monthly averaged per gridbox and then averaged over the globe. In 2004 the monthly mean maps of SC-AAI show results in the expected range of -2 to -1 .

The L2-AAI, shown in purple, correlates well with the scientific residue, but note that the y-axis is shifted by +6. The correction factors used to correct the reflectances to compute the SC-AAI cause a linear shift of the residue. The differences that remain between the SC-AAI and L2-AAI are due to the neglect of the polarisation in the Rayleigh atmosphere calculations and different sensitivities to processor changes.

An example of SCIAMACHY SC-AAI measurements is given in Fig. 3, which shows the SC-AAI on 16 June 2004. The daily global coverage of SCIAMACHY is illustrated, which is only 1/6th of the globe. The black rectangles are the outlines of the nadir states. Only within these states can an AAI be derived. This resolution makes daily monitoring of aerosols difficult, but the data is provided daily to offer the best possible resolution to end-users. The irregularly spaced orbits show that not all orbits were available, which was often the case (see Fig. 2, lower panel).

On 16 June 2004 desert dust aerosols can be found over northern Africa, the Middle East region, and parts of China, which are very common in these areas in June. Over the northern Atlantic low SC-AAI values can be observed in a number of states, with clear parts in the east pixels of some states. These are desert dust plumes extending over the Atlantic, with sun glint (see below) pixels removed from the data. Also over the Mediterranean Sea and the northern Pacific some remnants of sun glint can be observed.

4.1 Sun glint

Sun glint is a problem that occurs throughout the year. Sun glint generates a high SC-AAI signal in the eastern pixels of SCIAMACHY. If the sun glint angle is defined as the angle for which sun glint would occur if an ocean was a perfect mirror, the deviation from this angle $\Delta\Omega_{\text{glint}}$ can be defined for each pixel as

$$\cos(\Delta\Omega_{\text{glint}}) = \cos\theta_0 \cos\theta + \sin\theta_0 \sin\theta \cdot \cos(\phi - \phi_0). \quad (6)$$

Because the roughness of the oceans spreads out the sun glint signal, pixels having a sun glint deviation angle $\Delta\Omega_{\text{glint}}$ larger than zero can also be affected by sun glint. The geometrical sun glint condition was defined as the geometry for which the sun glint deviation angle was lower than 12° . A pixel satisfied the sun glint condition when it satisfied the geometrical sun glint condition and had an ocean as underlying surface. The underlying surface was determined using the $0.25^\circ \times 0.25^\circ$ GTOPO elevation database with an ocean flag. Pixels satisfying the sun glint condition were removed.

The residues of all pixels satisfying the sun glint condition of three months (October–December 2004) were compared to all land pixels satisfying the geometrical sun glint condition. The average residue of the sun glint pixels was -0.38 and that of the land pixels was -1.38 . The average residue for pixels not satisfying the geometrical sun glint condition was -1.56 over both land and ocean. This was considered

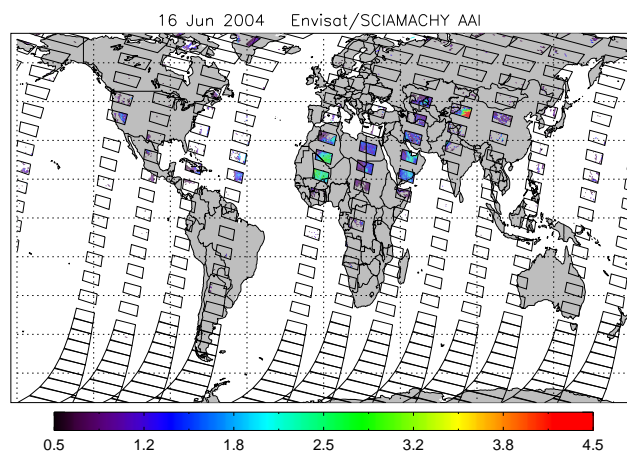


Fig. 3. Global SCIAMACHY SC-AAI on 16 June 2004. The black rectangles are the outlines of the nadir states.

a confirmation that the high residue in ocean sun glint pixels was anomalous and caused by sun glint.

The effect of using a sun glint deviation angle $\Delta\Omega_{\text{glint}}$ lower than 12° is illustrated in Fig. 4. Figure 4a shows the sun glint deviation angle for SCIAMACHY pixels on 12 December 2004 over the Indian Ocean, Indonesia and Australia, and the south-west Pacific. The pixels satisfying the sun glint condition are marked in red, other ocean pixels' sun glint deviation angles are marked according to the continuous colour scale. Figure 4b shows the SC-AAI when no sun glint mask is applied. Several bands with high SC-AAI values can be distinguished in the eastern pixels over the oceans, but not over land. Applying the 12° sun glint deviation angle mask removes most of the pixels with high signals (Fig. 4c). A more severe sun glint mask, e.g. removing all ocean pixels with sun glint deviation angles lower than 15° , improves the picture on 12 December 2004, because it is not likely that any aerosol events caused the high signals on this day in the area shown. But since the sun glint mask does not discriminate between sun glint and aerosol events, the sun glint mask will remove pixels with aerosol information for situations with aerosol plumes over the oceans. To reduce this problem the condition was set strict enough that sun glint is removed from most of the pixels, leaving only some small remnants in clear sky pixels with sun glint deviation angles close to 12° . These remnants will not easily be mistaken for artificial aerosol events. On the other hand, the condition is not so strict that it will remove all aerosol pixels from aerosol plumes over oceans. The locations of pixels satisfying the sun glint condition are easily recognised and the gaps which the sun glint mask produces are small enough so they will not greatly reduce the signal caused by aerosols.

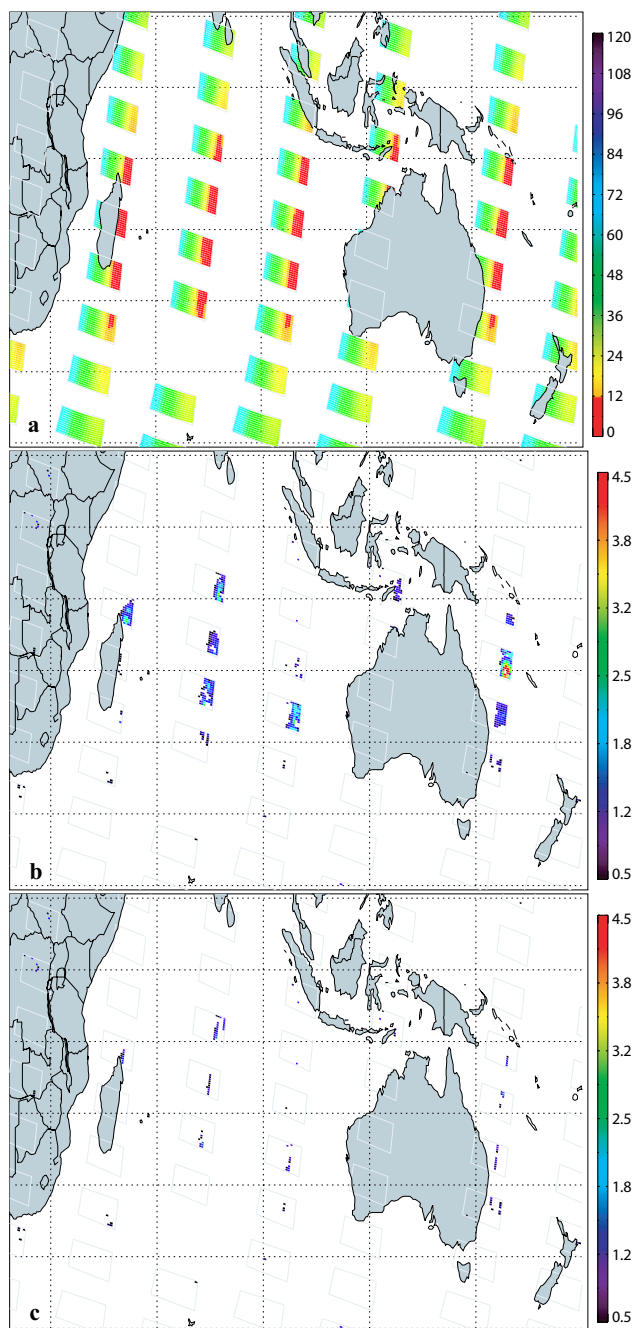


Fig. 4. SCIAMACHY SC-AAI on 12 December 2004 over the Indian Ocean, Indonesia and Australia, and the south-western Pacific. (a) Sun glint deviation angle of SCIAMACHY ocean pixels. The sun glint deviation angle has a smooth scale, but all pixels satisfying the sun glint condition, i.e. having a sun glint deviation angle lower than 12° , are marked in red. (b) SC-AAI without sun glint mask. (c) SC-AAI with all ocean pixels with a sun glint deviation angle lower than 12° removed.

4.2 Spatial and temporal patterns

Three-monthly means of SC-AAI in 2004 are presented in Fig. 5 to show the most persistent aerosol sources and seasonal variations. The range of the AAI data plotted in Fig. 5 is from -0.4 to 2.5 . Theoretically, for a well-calibrated AAI positive values should indicate absorbing aerosols. In reality some fine-tuning is needed to establish the right threshold. Figure 2 shows that the average of the scientific residue is about -2 , lower than the global average GOME residue in the period 1995–2000 (De Graaf et al., 2005), which was -1.2 . The correction factors for the SCIAMACHY reflectance offset are not entirely correct, causing the residue to be smaller than usual (see Sect. 4.4). Therefore, the lower plotting boundary was lowered to -0.4 .

The first panel of Fig. 5 is the average of the monthly means of January, February and December (JFD) of 2004. Only a few persistent aerosol sources over the Sahara show up in the plot. As was shown in Fig. 2, the average AAI in the first two months of 2004 was very low, probably due to incorrect calibration. Still, the southern part of the Sahara shows some signal.

The next panel in Fig. 5 shows the boreal spring (MAM) main aerosol sources. As was found with GOME (De Graaf et al., 2005), very persistent aerosol sources are found over northern Africa and the Middle East. SCIAMACHY also detects the aerosol plumes north-west of India, which were never detected by GOME because of its data storage problem in that region.

In the summer (JJA) the typical desert dust plume over the Sahara, extending far over the northern Atlantic, is clearly present. This is one of the most prominent features of the AAI and can be observed in all summer months. Also the biomass burning aerosol plume west of Angola, that was found every summer of 1995–2000 by GOME, is present. The aerosol plumes over the northern Sahara and the Middle East are strongest and most persistent, as a result of the most northerly position of the Inter-Tropical Convergence Zone (ITCZ) at that moment.

In autumn (SON) all aerosol plumes present in the summer are weaker, but still discernible. A clear plume is visible over the north-west of Australia. This plume frequently showed up in the GOME data as well, but was difficult to distinguish from the noise, because of the large footprint of GOME ($40 \times 320 \text{ km}^2$). SCIAMACHY data however clearly show a persistent aerosol source in this area. Possible sources might be desert dust from Australia or biomass burning from Indonesia and Australia or both.

4.3 Comparison with TOMS AAI

The SCIAMACHY SC-AAI was compared to the TOMS AAI. However, the TOMS AAI is different from the SCIAMACHY AAI in several ways. The definition of the TOMS AAI has changed with the introduction of version 8 data

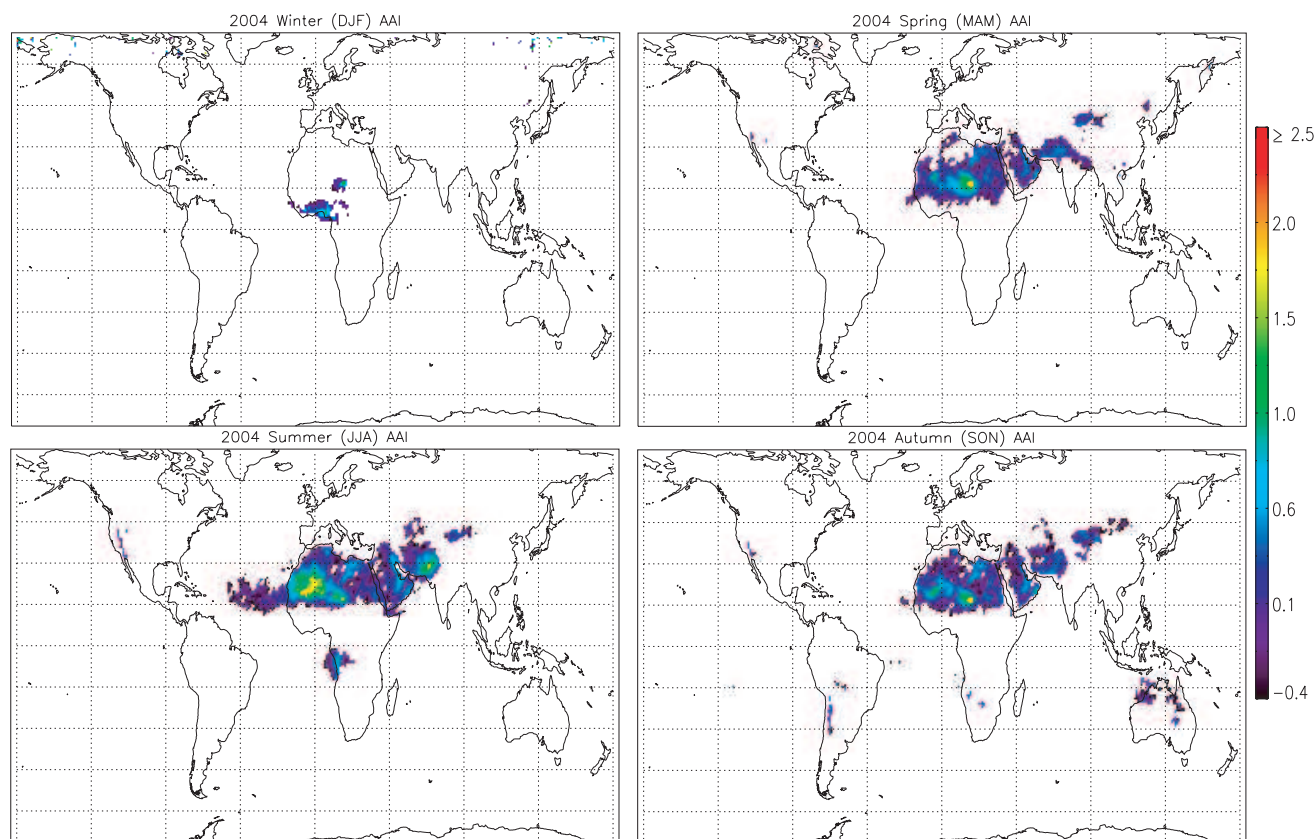


Fig. 5. Maps of the seasonally averaged global SC-AAI. Shown are the mean SC-AAI in January, February and December of 2004 (Winter), mean SC-AAI in March, April and May 2004 (Spring), mean SC-AAI in June, July and August 2004 (Summer) and mean SC-AAI in September, October and November 2004 (Autumn).

(2004), which has increased the sensitivity of the TOMS index, compared to that of version 7 data. This fact is not very widely known, but has quite large implications for the interpretation of the index. Also, the calibration differences of the instruments have an impact on the behaviour of the indices. Before the indices are compared, the different definitions are given and the differences in sensitivities will be highlighted.

Two wavelengths in the UV are used to calculate the AAI (Eq. 1). In the definition of the V7 TOMS AAI (also used for SCIAMACHY), the reference wavelength λ_0 is the largest of the two wavelengths (360 nm for TOMS and 380 nm for SCIAMACHY). In the definition of the V8 TOMS AAI this has changed and the reference wavelength is the shortest wavelength (331 nm for TOMS). This has increased the sensitivity of the index, see Fig. 6 where the monthly averaged TOMS V8 AAI is compared to the monthly averaged TOMS V7 AAI. The V8 AAI is about 1.5–2 times as sensitive as the V7 AAI and correlates nonlinearly. Also the V7 AAI was valid only from 0.7 upward, to indicate the presence of absorbing aerosols, in V8 this threshold has changed to zero (P. K. Bhartia, pers. comm.). Note that the majority of the points in Fig. 6 are on the line where V7 TOMS AAI is zero.

In the V7 definition this meant that there would be no absorbing aerosols, while all V8 pixels with AAI larger than zero now do indicate absorbing aerosols.

The reason for the increased sensitivity is the larger optical thickness at the lower wavelength (about 60% larger at 331 nm compared to 360 nm). In the AAI method all atmospheric scattering and absorbing effects are modelled with an adjusted surface albedo under a Rayleigh atmosphere. At the lower wavelength the atmospheric effects are relatively larger and the retrieved surface albedo is affected more strongly. The relationship between the V7 and the V8 AAI is nonlinear, because the reflectivity at the reference wavelength is a nonlinear function of geometry and atmospheric conditions. Nonlinear relationships between AAI with different reference wavelengths were also found by De Graaf et al. (2005).

Also note that the sensitivity of the TOMS AAI changes with the different TOMS instruments since different instruments had different channels. Currently, EP/TOMS uses channels in the UV at 331 nm and 360 nm. Before this (i.e. data from before 1996), TOMS instruments had channels in the UV at 340 nm and 380 nm. The same is true for GOME and SCIAMACHY; for GOME the wavelengths used were

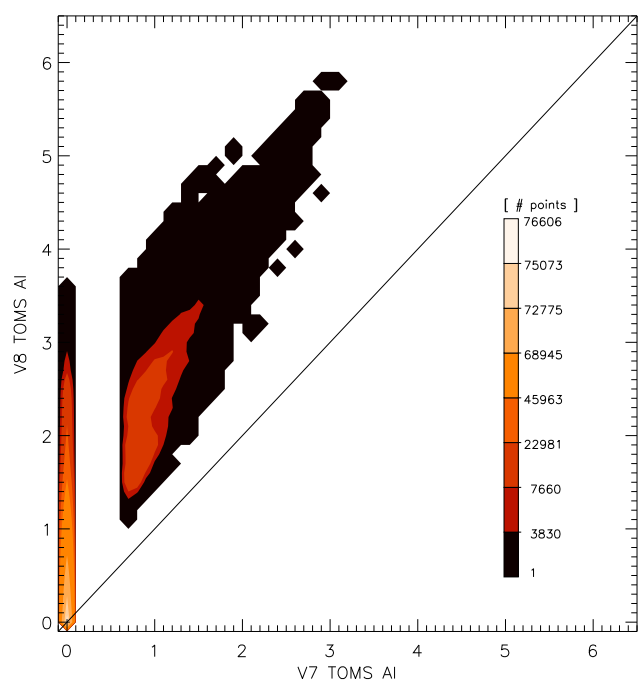


Fig. 6. Comparison of monthly averaged TOMS V7 AAI and TOMS V8 AAI, for all valid points in the period January 2002–July 2003. TOMS V7 AAI is only defined for values >0.7 .

335 nm and 380 nm and for SCIAMACHY the wavelengths were 340 nm and 380 nm, but as long as the reference wavelength is unchanged the relationship is linear.

Note that all TOMS AAI data from 1978 to present are reprocessed according to the V8 definition. So all the data presently available on the Internet are 1.5–2 times as sensitive as those published in papers so far. The definition of SCIAMACHY AAI is the same as the original TOMS V7 AAI, so the results from SCIAMACHY (and also its predecessor GOME) are comparable with TOMS V7 AAI and the results of the papers that explain and investigate the sensitivity of the AAI (Herman et al., 1997; Torres et al., 1998; De Graaf et al., 2005).

4.4 Zonal patterns

The performance of the SC-AAI was compared to TOMS data, see Fig. 7. In this figure the zonal averages of the SCIAMACHY residue (black bold solid line), the SCIAMACHY AAI (black normal solid line), the TOMS V7 residue (purple dashed line), the TOMS V7 AAI (green dashed-dotted line), and the TOMS V8 AAI (red dotted line) are plotted, for 2002, 2003, and 2004. The TOMS V7 residues are daily values, the TOMS V7 AAI are monthly averages. These V7 products are no longer available, because the data are replaced by V8 data, but the V7 products in the figure had been saved from previous studies. The monthly averaged TOMS V7 AAI were only available from January 2002 to July 2003, the daily TOMS

V7 residues were available from January 2002 to June 2004. All other other products are freely available for the periods that the various instruments produced measurements. The SCIAMACHY data is cut-off above 60° N and S. Zero values (and invalid data) are not plotted, hence the curves do not always extend to the poles.

The differences between the TOMS V7 residue (purple dashed line) and the TOMS V7 AAI (green dashed-dotted line) show the behaviour of averaging a quantity that is defined by a threshold. Since only TOMS V7 residues larger than 0.7 are defined as TOMS V7 AAI, the averaged TOMS V7 AAI is always positive and the zonal structure of the AAI is different from the zonal structure of the residue because the number of points over which is averaged is not constant for the AAI (it is not always defined). The same holds for the SCIAMACHY AAI (black normal solid line) and the SCIAMACHY (black bold solid line) residue. Since the calibration of SCIAMACHY is different from that of TOMS the threshold from which to define the AAI is different and comparison of the AAI is difficult. Instead we compare residues (SCIAMACHY and TOMS V7), because an error in the calibration in one or both instruments will only yield a different absolute value of the residue (assuming the sensitivity of the residue to the geometry and atmospheric conditions is the same). Of the version 8 data only AAI data are provided in the TOMS L3 datasets. The full residuals are provided on the TOMS L2 datasets but these were not investigated.

In 2002 the SCIAMACHY residue (and hence SC-AAI) results are not very satisfactory, no clear zonal pattern is discernible in Fig. 7. In 2003 a local peak is seen around 25° N, but the picture is mostly determined by the noise near the poles. In 2004 the noise level has dropped below the signal level and is confined to a region near 60° N and S. The SCIAMACHY residue correlates well to the TOMS V7 residue in 2004, although the SCIAMACHY residue is lower by about 0.2. The SCIAMACHY residue correlates also well with the TOMS V8 AAI in 2004 (but shifted by -0.4).

A clear peak in the SCIAMACHY residue can be distinguished between 5° – 30° N, which is where the major Northern Hemisphere (NH) deserts are located. A smaller peak can be found on the Southern Hemisphere (SH), between 0° – 30° S. The TOMS V7 AAI shows the same behaviour, although the relative differences between the NH and SH are less than in the SCIAMACHY residue. In the period 1996–2000 both TOMS and GOME found a similar behaviour, with a large difference between the NH and SH (De Graaf et al., 2005).

From the difference between the SCIAMACHY and TOMS V7 residues we might conclude that the quotient of the correction factors is not correct, producing smaller residues than expected. Therefore the threshold where absorbing effects and scattering effects are separated, and from which the AAI must be defined, is smaller than that of TOMS, probably even negative. Whether the correction factor for the smallest wavelength (R_{340}) is too large or

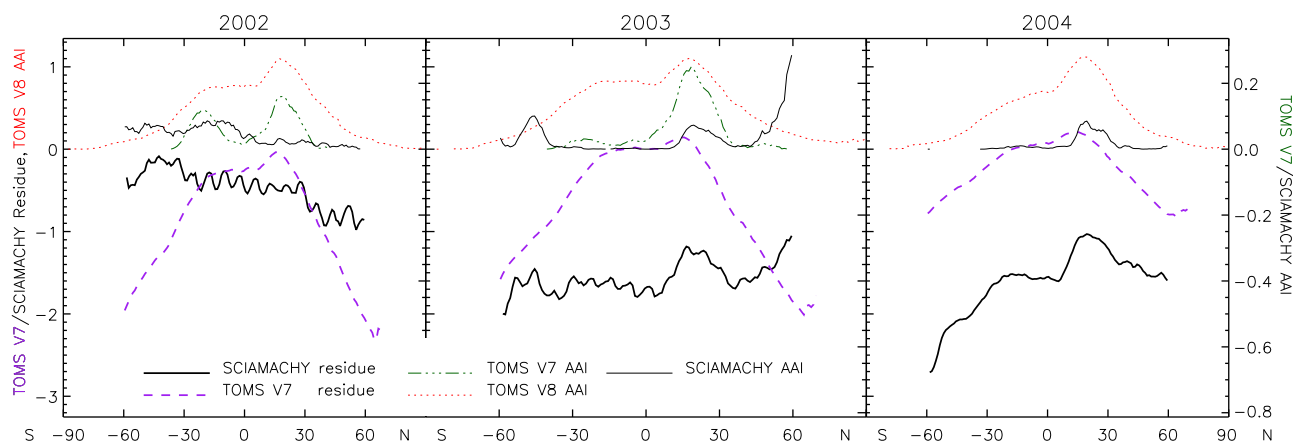


Fig. 7. Zonal average of SCIAMACHY residue (black bold solid line), SCIAMACHY AAI (black normal solid line), TOMS V7 residue (purple dashed line), TOMS V7 AAI (green dashed-dotted line), and TOMS V8 AAI (red dotted line), for 2002–2004. Left y-axis refers to the TOMS and SCIAMACHY residues and the TOMS V8 AAI, the right y-axis refers to the SCIAMACHY and TOMS V7 AAI.

the correction factor for the largest wavelength (R_{380}) is too small cannot be determined, because the residue only gives information about the slope of the reflectance spectrum. From the value of -0.2 between SCIAMACHY and TOMS V7 residues we can conclude the error in the quotient of the correction factors is about 0.5 – 1 %. The TOMS V8 AAI is larger than the SCIAMACHY residue by about 0.4 , but this additional value is caused TOMS' higher sensitivity and greater daily global coverage. When more positive values are found the (zonal) average will increase since the number of pixels over which is averaged will increase.

5 Conclusions

The scientific Absorbing Aerosol Index product (SC-AAI) of SCIAMACHY shows promising results for 2004. The underestimated reflectance of SCIAMACHY in the UV (Tilstra et al., 2004) was corrected with constant multiplication factors at the AAI wavelengths 340 nm (1.210) and 380 nm (1.130). This resulted in an AAI that is almost in the expected range of lower than zero for scattering events (clouds and scattering aerosols) and higher than zero for absorbing aerosols. However, Figs. 5 and 7 show that the correction factors are still not correct and a better calibration of the reflectances is necessary. The error in the quotient of the correction factors is about 0.5 – 1 %.

The SC-AAI algorithm accounts for polarisation in the Rayleigh reflectances, thereby improving the viewing angle offset found in the operational AAI product (L2-AAI). As the L2-AAI is calculated in the level 1 to level 2 processing stage, the LUTs used by the processor can easily be updated using a radiative transfer model incorporating (linear) polarisation. This would improve the L2-AAI and make it a useful product. The only problem remaining then for the op-

erational product would be the reflectance offset, which can be corrected using a linear shift of the AAI. This change of LUTs is highly recommended.

The SCIAMACHY SC-AAI has revealed sun glint related problems in the interpretation of the AAI. Sun glint can easily be defined geometrically, but the sun glint mask used for SCIAMACHY pixels does not distinguish between high AAIs as a result from sun glint or from aerosol events. This might be improved using the absolute value of the reflectances. Absorbing aerosol events reduce the reflectances, but more so at the lower wavelength, causing a positive residue. It is anticipated that sun glint will increase the reflectances, but probably more so at the higher wavelength, also creating a positive residue.

The SC-AAI gives reasonable results after March 2004, when the processor version was updated to version 5.01. The seasonal means in 2004 show the same characteristics as were found by GOME in 1995–2000 and the same as found by TOMS. This makes SCIAMACHY suitable for the continuation of the long-term AAI record, now that GOME is failing and EP/TOMS is suffering from degradation.

Acknowledgements. L. G. Tilstra is thanked for his many helpful contributions to this paper. NASA GSFC is acknowledged for the use of their data. This work was financed by the Netherlands Agency for Aerospace Programmes (NIVR) SCIAMACHY validation project.

Edited by: P. C. Simon

References

- Alpert, P. and Ganor, E.: Sahara mineral dust measurements from TOMS: Comparison to surface observations over the Middle East for the extreme dust storm, 14–17 March 1998, *J. Geophys. Res.*, 106, 18 275–18 286, 2001.

- Balzer, W., Spurr, R., Thomas, W., Kretschel, K., and Bollner, M.: SCIAMACHY level 1b to 2 NRT Processing Input/Output Date Definition, Tech. Rep. ENV-TN-DLR-SCIA-0010, Issue 3/B, Dtsch. Zent. für Luft- und Raumfahrt, Oberpfaffenhofen, Germany, 2000.
- Bovensmann, H., Burrows, J. P., Buchwitz, M., Frerick, J., Noël, S., Rozanov, V. V., Chance, K. V., and Goede, A. P. H.: SCIAMACHY: Mission Objectives and Measurement Modes, *J. Atmos. Sci.*, 56, 127–150, 1999.
- Chandrasekhar, S.: Radiative Transfer, Dover, Mineola, N. Y., 1960.
- Chiapello, I., Prospero, J. M., Herman, J. R., and Hsu, N. C.: Detection of mineral dust over the North Atlantic Ocean and Africa with the Nimbus 7 TOMS, *J. Geophys. Res.*, 104, 9277–9291, 1999.
- Darmenova, K., Sokolik, I. N., and Darmenov, A.: Characterization of east Asian dust outbreaks in the spring of 2001 using ground-based and satellite data, *J. Geophys. Res.*, 110, D02204, doi:10.1029/2004JD004842, 2005.
- De Graaf, M. and Stammes, P.: First verification of SCIAMACHY's Absorbing Aerosol Index product, in: Envisat Calibration Review Proceedings, ESA Special publication SP-531, 2002.
- De Graaf, M., Tilstra, L. G., and Stammes, P.: SCIAMACHY absorbing aerosol index: the scientific product compared to the operational product and TOMS data, in: Proceedings of the Second Workshop on the Atmospheric Chemistry Validation of ENVISAT (ACVE-2), ESA Special publication SP-562, 2004.
- De Graaf, M., Stammes, P., Torres, O., and Koelemeijer, R. B. A.: Absorbing Aerosol Index: Sensitivity Analysis, application to GOME and comparison with TOMS, *J. Geophys. Res.*, 110, D01201, doi:10.1029/2004JD005178, 2005.
- De Haan, J. F., Bosma, P. B., and Hovenier, J. W.: The adding method for multiple scattering calculations of polarized light, *Astron. Astrophys.*, 183, 371–391, 1987.
- Duncan, B. N., Bey, I., Chin, M., Mickley, L. J., Fairlie, T. D., and Martin, R. V.: Indonesian wildfires of 1997: Impact on tropospheric chemistry, *J. Geophys. Res.*, 108, D154458, doi:10.1029/2002JD003195, 2003.
- Gleason, J. F., Hsu, N. C., and Torres, O.: Biomass burning smoke measured using backscattered ultraviolet radiation: SCAR-B and Brazilian smoke interannual variability, *J. Geophys. Res.*, 103, 31 969–31 978, 1998.
- Herman, J. R., Bhartia, P. K., Torres, O., Hsu, C., Seftor, C., and Celarier, E. A.: Global distributions of UV-absorbing aerosols from NIMBUS 7/TOMS data, *J. Geophys. Res.*, 102, 16 911–16 922, 1997.
- Hsu, N. C., Herman, J. R., Bhartia, P. K., Seftor, C. J., Torres, O., Thompson, A. M., Gleason, J. F., Eck, T. Y. F., and Holben, B. N.: Detection of biomass burning smoke from TOMS measurements, *Geophys. Res. Lett.*, 23, 745–748, 1996.
- Hsu, N. C., Herman, J. R., Gleason, J. F., Torres, O., and Seftor, C. J.: Satellite Detection of Smoke Aerosols Over A Snow/Ice Surface By TOMS, *Geophys. Res. Lett.*, 26, 1165–1168, 1999.
- Moulin, C. and Chiapello, I.: Evidence of the control of summer atmospheric transport of African dust over the Atlantic by Sahel sources from TOMS satellites (1979–2000), *Geophys. Res. Lett.*, 31, L02107, doi:10.1029/2003GL018931, 2004.
- Pandithurai, G., Pinker, R. T., Dubovik, O., and Aro, T. O.: Remote sensing of aerosol optical characteristics in sub-Sahel, West Africa, *J. Geophys. Res.*, 106, 28 347–28 356, 2001.
- Prospero, J. M., Ginoux, P., Torres, O., Nicholson, S. E., and Gill, T. E.: Combined use of satellite and surface observations to infer the imaginary part of the refractive index of Saharan dust, *Rev. Geophys.*, 40, 1002, doi:10.1029/2000RG000095, 2002.
- Spichtinger, N., Wenig, M., James, P., Wagner, T., Platt, U., and Stohl, A.: Satellite detection of a continental-scale plume of nitrogen oxides from boreal forest fires, *Geophys. Res. Lett.*, 28, 4579–4582, 2001.
- Spurr, R. and Balzer, W.: SCIAMACHY level 1c to 2 Off-line Processing. Algorithm Theoretical Basis Document, Tech. Rep. ENV-ATB-SAO-SCI-2200-0003, Issue 2, Dtsch. Zent. für Luft- und Raumfahrt, Oberpfaffenhofen, Germany, 2000.
- Spurr, R. J. D., Kurosu, T. P., and Chance, K. V.: A Linearized discrete Ordinate Radiative Transfer Model for Atmospheric Remote Sensing Retrieval, *J. Quant. Spectrosc. Radiat. Transfer*, 68, 689–735, 2001.
- Tilstra, L., van Soest, G., de Graaf, M., Acarreta, J., and Stammes, P.: Reflectance comparison between SCIAMACHY and a radiative transfer code in the UV, in: Proceedings of the Second Workshop on the Atmospheric Chemistry Validation of ENVISAT (ACVE-2), ESA Special publication SP-562, 2004.
- Torres, O., Bhartia, P. K., Herman, J. R., Ahmad, Z., and Gleason, J.: Derivation of aerosol properties from satellite measurements of backscattered ultraviolet radiation: Theoretical basis, *J. Geophys. Res.*, 103, 17 099–17 110, 1998.